Combined theoretical and experimental investigation of the adsorption geometry of Ga on Si(100) at low coverage

Shaoping Tang and A. J. Freeman
Materials Research Center, Northwestern University, Evanston, Illinois 60208
and Department of Physics and Astronomy, Northwestern University, Evanston, Illinois 60208

Yonglin Qian
Materials Science Division, Argonne National Laboratory, Argonne, Illinois 60439
and Department of Materials Science and Engineering, Northwestern University, Evanston, Illinois 60208

Gregg E. Franklin
Department of Physics, Harvard University, Cambridge, Massachusetts 02142

Michael J. Bedzyk
Materials Research Center, Northwestern University, Evanston, Illinois 60208;
Materials Science Division, Argonne National Laboratory, Argonne, Illinois 60439;
and Department of Materials Science and Engineering, Northwestern University, Evanston, Illinois 60208
(Received 11 July 1994)

The atomic and electronic structures of Ga chemisorption on the Si(100)-(2×1) at low coverage have been investigated by a combined molecular-cluster total-energy and atomic-force approach and x-ray standing-wave (XSW) measurements. Four possible Ga-dimer adsorption geometries are calculated using cluster models with up to 77 atoms. By comparing the total energies for these optimized geometries, it is found that Ga dimers are centered at valley bridge sites with the Ga-dimer bond oriented parallel to the underlying Si-dimer bonds—a geometry strongly supported by XSW measurements of the Si(100)-(2×2)-Ga surface structure. The calculated Ga-dimer height above the ideal Si(100) is in excellent agreement with the XSW result. The stability of this parallel-dimer model is explained through the bonding between Ga-Si and Si-Si and by analyzing the Si-surface distortion when Ga is present.

I. INTRODUCTION

Structural studies of clean and metal-covered Si(100) surfaces and interfaces have long been the subject of interest for both scientific and technological reasons. The clean Si(100)-(2×1) surface is known to form dimers that reduce the number of dangling bonds on the ideal surface.[1] Adsorption of metal atoms can further saturate the Si dangling bonds and form new reconstructed structures. These surfaces phases, which are a result of chemical bonding between the adatoms and the surface Si atoms, may play an important role in the epitaxial growth of metals and semiconductor thin films on Si(100). Thus it is highly desirable to understand these structures and how they form.

The adsorption of group-III metals (e.g., Al, Ga, and In) on Si(100)-(2×1) (Refs. 2–14) has recently received considerable attention. This group of metals induces on Si(100) an abundance of surface reconstructions, such as 2×3, 2×5, 2×2, and 1×8; most of these reconstructions occur at coverages below one-half monolayer (ML) (where 1 ML=6.78×10^{14} atoms/cm^2). These structures have been studied experimentally by reflection high-energy electron diffraction (RHEED),[3] low-energy electron diffraction (LEED),[4,5] Auger electron spectroscopy (AES),[4,5] and scanning tunneling microscopy (STM).[6–8] In their LEED study of Ga/Si(100), Bourguignon, Carleton, and Leone[4] proposed a structural model, shown in Fig. 1(a), for interpreting the low-coverage surface phases. This model assumes that the Ga ad-dimers lie between adjacent Si-dimer rows and are oriented orthogonal to the Si-dimer bond. The spacing of these Ga ad-dimer rows can be arranged to form 2×3, 2×5, and 2×2 phases at coverages of $\frac{1}{3}$, $\frac{2}{5}$, and $\frac{1}{2}$ ML, respectively. The STM study of Ga/Si(100) by Nogami and co-workers[6–8] observed both the 2×3 and 2×2 structures when Ga coverages were below 0.5 ML. Later, the same authors found for the related Al/Si(100) system[9] that, in addition to the orthogonal ad-dimer model, a parallel ad-dimer model, illustrated in Fig. 1(b), is also consistent with the STM images and the LEED pattern. A recent impact-collision ion-scattering spectrometry (ICISS) experiment by Steel and co-workers[10] of In/Si(100) found that at low coverage In forms parallel ad-dimers. The most recent STM study of Al/Si(100) by Itoh and co-workers[11] also confirms the parallel ad-dimer model.

On the theoretical side, three pseudopotential total-energy calculations have been performed for group-III metals adsorbed on Si(100). Batra[12] studied Al- and Ga-dimer adsorption on Si(100) and suggested that the underlying Si dimers are broken at coverages above 0.5 ML. The parallel ad-dimer model was not examined in that paper. Northrup and co-workers[13] determined from their total-energy calculations that the parallel metal ad-dimer

is more stable than the orthogonal ad-dimer model. For the Si(100)-(2×2)-Ga surface, they obtained quite a large energy difference of 1.32 eV per atom between the parallel ad-dimer and the orthogonal ad-dimer. A recent pseudopotential calculation by Brocks, Kelly, and Car for the Al/Si(100) surface[14] also supported the parallel ad-dimer model.

It thus appears that group-III metals adsorbed on Si(100)-(2×1) establish a unique structural feature by forming parallel metal dimers on the surface. Elements of other groups such as Ge, As, and Sb are known to have orthogonal dimers on Si(100).[15–19] Until now, quantitative experimental measurements of the adsorption structure of group-III metals on Si(100) were lacking and the reason why the parallel dimer is more stable than the orthogonal dimer was unclear.

In this paper we report results of a combined theoretical and experimental determination of Ga adsorption geometries on Si(100)-(2×1) at coverages below 0.55 ML. Using a first-principles molecular-cluster approach, called "DMol," we have investigated four different Ga ad-dimer structure models shown in Fig. 2. Experimentally, we have studied the Si(100)-(2×2)-Ga surface structure with (400) and (220) x-ray standing-wave (XSW) measurements. This experiment represents a high-resolution quantitative measurement for Ga chemisorbed on the Si(100)-(2×1) surface. By comparing the adsorption energies of these four structures, the most stable structure was found to be the parallel dimer at the valley bridge site (PV model in Fig. 2). This dimer model was further confirmed by the excellent agreement between the calculated Ga-dimer height above the ideal Si(100) surface and the experimental measured value. By analyzing the atomic and electronic structures of parallel and orthogonal dimers at the valley bridge site, it is found that the Ga parallel dimers induce considerably less distortion than the orthogonal dimers. The Ga-Si and Si-Si bonding is stronger in the parallel dimer structure than in the orthogonal dimer structure. These factors contribute to the stability of the parallel dimer structure.

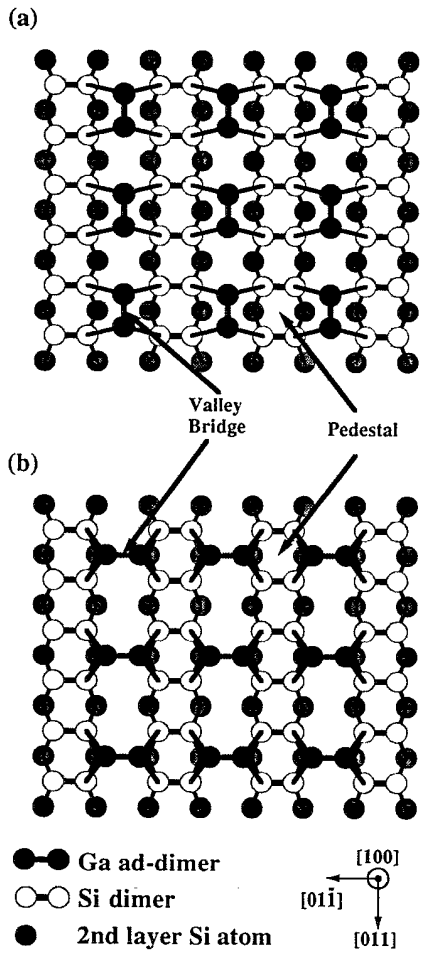

FIG. 1. Top view of 2×2 Si(100) metal ad-dimer surface models: (a) orthogonal dimer model at the valley bridge site; (b) parallel dimer model at the valley bridge site.

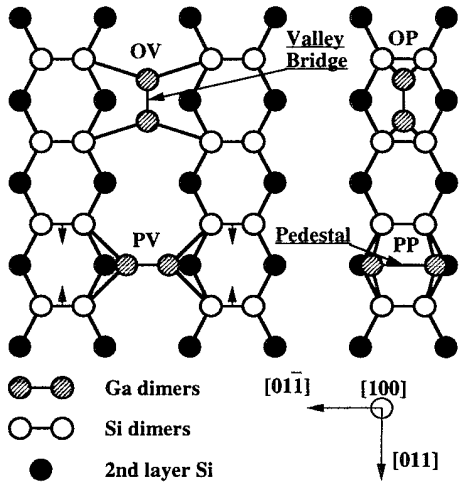

FIG. 2. Top view of four possible Ga-dimer structures on Si(100)-(2×1): orthogonal dimer model at the valley bridge site (OV) and at pedestal site (OP), and parallel dimer at valley bridge site (PV) and at pedestal site (PP).

II. THEORETICAL APPROACH

For the theoretical calculations, we employ the DMol method.[20] This is a first-principles molecular-cluster approach based on the local-density approximation to density-functional theory. The detailed formalism for the DMol method and the calculation of energy derivatives were presented by Delley.[20,21] Here, we describe some details pertinent to our calculation. We used an extended double numerical basis set for Ga and Si that contains a double set of valence functions plus a single *d* polarization function and a double numerical basis for H. The extended double numerical basis set has proven to be very reliable in studying metal adsorption on Si(100)-(2×1) (Ref. 19) and other molecular systems.[20,21] The frozen-core approximation was used for Ga and Si except that the Ga 3*d* electrons were treated fully in the self-consistent iterations. The Hedin-Lundqvist[22] exchange-correlation potential was adopted in the calculations.

For simulating the bare Si(100)-(2×1) reconstructed surface, we used a symmetric dimer arrangement[23] previ-

ously found to relax the first-layer Si atoms inward by 0.38 Å and a dimer bond length of 2.23 Å. Several clusters of different sizes which were used to simulate the Si(100)-(2×1) surfaces are described in the next section. As usual, hydrogen atoms were used to saturate the Si dangling bonds at the cluster boundary and the Si-H bond length was taken to be 1.48 Å.

The binding energy of a cluster is defined as

$$E_b = E_t - E_a \ , \tag{1}$$

where the E_a is the sum of atomic energies and E_t is the total energy of the cluster. For the chemisorption problem, the difference between the binding energy of a cluster of the clean surface and a cluster of the chemisorbed surface, i.e., the chemisorption energy, is given by

$$\Delta E = E_b(\text{chemisor.}) - E_b(\text{clean}) \ . \tag{2}$$

A negative ΔE value means a possible chemisorption system. Obviously, the lower the chemisorption energy, the more stable the system. In practice, the binding energy of a given geometry and the atomic force on selected atoms are calculated. To find optimized atomic positions, atoms are moved along the force direction until the forces acting on them are sufficiently small. The force convergence criterion is taken to be 4.0×10^{-3} Ry/a.u. The degree of convergence of the self-consistent iterations, measured by root mean square (rms) changes in the charge density, is set to 10^{-6} which allows the total energy to converge to 10^{-6} Ry.

III. THEORETICAL RESULTS

Let us first examine the adsorption sites for Ga dimers. The orthogonal and parallel dimer models proposed in the literation (shown in Fig. 1) both have the mass center of the Ga dimer above the valley bridge site but with different orientations for the Ga dimer relative to the Si-dimer bond. At the valley bridge site, each Ga atom bonds with three nearest-neighbor atoms, which is consistent with its three valence electrons. Another possible adsorption site that complies with Ga valence considerations is the pedestal site shown in Fig. 1, which has not been studied theoretically for the Ga/Si system. Thus, counting the two dimer orientations at each site, there are four Ga-dimer configurations shown in Fig. 2 that must be considered as possible adsorption geometries. The simulation of these geometries is accomplished by using the two cluster models displayed in Fig. 3, where only the parallel dimer arrangement is shown. Each cluster includes Si atoms up to the fifth layer. The orthogonal dimers can be studied by rotating the dimer by 90° and keeping the dimer mass center at valley bridge or pedestal sites.

For each dimer configuration, we calculated the adsorption energy by varying the distance between Ga and the Si surface and the distance between Ga and Ga atoms until the minimum energy is found. By calculating forces (energy gradients) on Ga atoms, the direction of the required movement of the Ga atoms is easily determined. Assuming a rigid substrate, the calculated adsorption energies and height of the Ga dimer above the ideal Si(100)-(1×1) plane for each dimer geometry are presented in Table I. As can be seen from this table, the adsorption energy of the parallel dimer at the valley bridge site (PV) is much lower than that of the three other structures, and is thus the most stable structure energetically. This is in agreement with the pseudopotential result.[13]

It is known that metal adsorption on Si can induce large relaxations of the Si substrate;[24] hence, a complete study of Ga dimers on Si(100) should consider the relaxation of the substrate. To this end, the larger cluster shown in Fig. 4 consisting of 39 Si, 32 H (not shown in this figure), and 4 Ga atoms was employed to calculate the parallel Ga-dimer structure at the valley bridge site (PV). We put a Ga dimer on the surface center and two Ga atoms at the surface boundary in order to simulate the environment of neighboring dimers. The first three Si layers were allowed to relax while the fourth and fifth layers were fixed in their bulk positions. C_{2V} symmetry was kept for the cluster during the relaxation studies. For comparison with the pseudopotential calculation,[13] we also carried out relaxation studies for the orthogonal dimer at the valley bridge site (OV). The cluster used for this dimer is similar to that shown in Fig. 4 but with the parallel dimer rotated by 90° and the two boundary Ga atoms replaced with two pairs of orthogonal Ga dimers. The final optimized results are listed in Table II along with the pseudopotential results[13] and our x-ray standing-wave measurement described in Sec. V. It can be seen from the table that the height calculated by DMol of the Ga parallel dimer relative to the ideal surface (i.e., h') is very close to the experimental result.

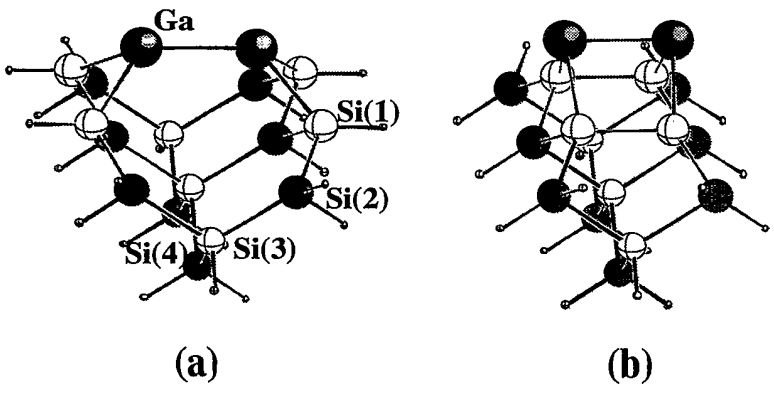

FIG. 3. Two cluster models used to simulate the Ga dimers at valley bridge and pedestal sites. Only the parallel dimers are shown here. (a) $Ga_2Si_{15}H_{20}$ cluster; (b) $Ga_2Si_{15}H_{16}$ cluster.

TABLE I. The adsorption energy E_{ad} and Ga-dimer height h' above the ideal Si(100)-(1×1) surface for Ga/Si(100)-(2×1) using cluster models depicted in Fig. 3.

	OV	OP	PV	PP
E_{ad} (eV/atom)	−3.14	−3.29	−4.15	−3.43
h' (Å)	0.69	1.64	1.10	1.27

TABLE II. Optimized structural parameters (in Å) for Ga dimers on Si(100)-(2×1): h is the vertical height of the Ga dimer from the Si(100)-(2×1) surface, and $L_{Si\text{-}Si}$, $L_{Ga\text{-}Si}$, and $L_{Ga\text{-}Ga}$ stand for Si-dimer, Ga-Si, and Ga-dimer bond lengths, respectively. Δz represents the inward relaxation of the top Si layer relative to the bulklike position and Δy is the lateral movement of the Si-dimer atoms along the [011] direction indicated by arrows in PV model of Fig. 2. h' is the height of the Ga dimer relative to the ideal surface.

	Parallel		Orthogonal		
	Present	Ref. 13	Present	Ref. 13	XSW
$L_{Si\text{-}Si}$	2.49	2.46	2.80	2.84	
$L_{Ga\text{-}Si}$	2.54	2.47	2.63	2.61	
$L_{Ga\text{-}Ga}$	2.65	2.63	2.64	2.50	2.50±0.06
h	1.18	1.09	0.77	0.73	
Δz	0.13	0.17	0.08	0.13	
Δy	0.07		0.00		
$h'=h-\Delta z$	1.05	0.92	0.69	0.60	1.03±0.02

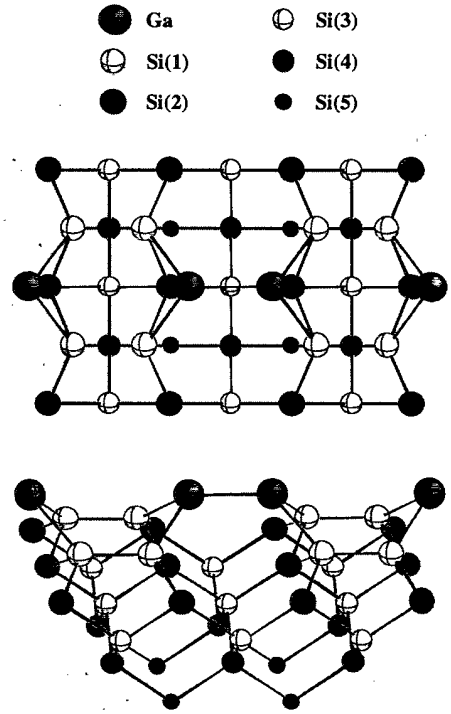

FIG. 4. The $Ga_4Si_{39}H_{32}$ cluster model used to simulate the parallel dimer at the valley bridge site. This is given in top view from the [100] direction and side view from the [011] direction, and the hydrogen atoms are not shown.

IV. X-RAY STANDING-WAVE TECHNIQUE

When an incident x-ray plane wave is Bragg diffracted by a perfect single crystal, the interference between the incident and reflected plane wave generates an x-ray standing wave inside the crystal[25] and above the crystal surface[26] with a period equal to the d spacing of the Bragg diffraction planes.

As the incident angle is scanned in angle θ through the Darwin width for strong Bragg reflection, the nodes and antinodes of the XSW move inward by one-half of a d spacing due to a π rad phase shift of the reflected plane wave. If the energy of the incident x ray is above the adsorption edge of an impurity atomic species, the fluorescence from that species is stimulated and is proportional to the electric-field intensity of the XSW at the center of the impurity atom. Therefore, the phase shift of the XSW will give rise to a characteristic modulation of the fluorescence emission from adatoms on the crystal surface. The θ dependence of the normalized fluorescence yield from a distribution of adatoms can be expressed as

$$Y(\theta)=1+R(\theta)+2[R(\theta)]^{1/2}f_{c,H}\cos[v(\theta)-2\pi P_H]\ , \tag{3}$$

where $R(\theta)$ is the reflectivity and $v(\theta)$ is the relative phase of the reflected plane wave. The coherent fraction $f_{c,H}$ and coherent position P_H are, respectively, the amplitude and the phase of the Hth Fourier coefficient for the normalized adatom density distribution function. Unlike standard x-ray-diffraction techniques, which in general only measure the amplitude of the structure factor, the x-ray standing-wave method measures both the amplitude and the phase of the Fourier coefficient. The XSW has been developed as a high-precision probe for locating positions of adatoms at crystal surfaces.[15,26–29]

Based on the convolution theorem, the coherent fraction can be written as the product of three factors:[28]

$$f_{c,H}=Ca_HD_H\ . \tag{4}$$

The three factors, which range in value from zero to unity, are the ordered fraction C, the geometrical factor a_H, and the Debye-Waller factor $D_H=\exp(-2\pi^2\langle u_H^2\rangle/d_H^2)$; here $\langle u_H^2\rangle$ is the mean-square thermal vibrational amplitude of the adatom in the **H** direction, where $|\mathbf{H}|=1/d_{hkl}$. For the case of Ga forming symmetric (unbuckled) dimers on the Si(100) surface (see Fig. 1 and the inset in Fig. 5), the geometrical factor a_H is a measure of the projected separation of the two Ga adatoms along **H**. More specifically, the (400) and (220) geometrical factors can be written as

$$a_{400}=1\ ,\ \text{and}\ a_{220}=|\cos(\pi L/2d_{220})|\ , \tag{5}$$

where L is the ad-dimer bond length. The coherent position P_H indicates the location of the center of the Ga dimer along the **H** direction. For the [400] direction, $P_{400}=h'/d_{400}$, where h' is the height of the Ga dimer above the Si(400) bulklike lattice plane. If the center of the Ga ad-dimer is above one of the 2mm symmetry sites in Fig. 1, the value of P_{220} must be equal to $(1+P_{400})/2$.

It should be noted that the above formulas for the (400) and (220) values of a_H and P_H for either of the two models do not change when atomic steps are introduced.

V. EXPERIMENT

The experimental work was performed at the X15A beamline of the National Synchrotron Light Source at Brookhaven National Laboratory. The multichamber ultrahigh-vacuum (UHV) system at X15A allows for sample preparation, surface characterization, and x-ray measurements. (A detailed description of the experimental facilities at X15A can be found in Ref. 30.) Before insertion into the UHV chamber, the Si(100) samples were Syton™ polished and chemically etched by the Shiraki procedure.[31] The base pressure in the UHV system was 9×10^{-11} torr. After outgassing at 600 °C for 5×10 h, the sample was flash annealed to 900 °C for 10 min to remove the thin surface oxide layer. During the flash annealing, the chamber pressure went up to 10^{-9} torr temporarily but dropped immediately back to 10^{-10} torr. A sharp two-domain 2×1 LEED pattern for the clean Si surface was observed after the sample was cooled down to room temperature.

The Auger spectrum showed no trace of O and a small C peak on the surface corresponding to ~0.03 ML. Ga was then evaporated onto the Si from molecular-beam epitaxy effusion cell held at 840 °C with the Si substrate held at room temperature. This gave a Ga deposition rate of $(4-5)\times10^{-3}$ ML/sec. By using the ratio of the Ga to Si Auger peaks and Rutherford backscattering, the Ga coverage was calibrated to be directly proportional to the exposure time up to 1 ML, with a relative error of 10%. We have prepared the Ga/Si(100) surfaces with various Ga coverages ranging from 0.35 to 0.55 ML while the Si substrate was held at room temperature. For all of these coverages, we observed a 2×2 LEED pattern. We did not see the 2×3 or 2×5 LEED patterns reported in an earlier experiment.[4] The room-temperature STM study[7] also did not observe these LEED patterns.

We then transferred the prepared sample into another chamber in the UHV system where XSW measurements were performed. An XSW measurement consists of simultaneously recording the Darwin curve x-ray reflectivity, $R(\theta)$, from the single crystal and the adatoms' fluorescence yield $Y(\theta)$. The parameters $f_{c,H}$ and P_H are determined by a χ^2 fit of Eq. (3) to the experimentally measured adatom fluorescence yield data. For all coverages of the Ga/Si(100) surface mentioned above, XSW measurements using the (400) reflection were performed at room temperature. (220) measurements were also done for some of these coverages.

Table III lists the results of our XSW measured values for $f_{c,H}$ and P_H at various coverages. Figure 5 presents data for the (400) x-ray reflectivity and Ga $K\alpha$ fluorescence yield for the 0.50 ML of Ga measurement which was taken at an incident energy at 13.0 keV.

Using the results of the (400) and (220) measurements, we are able to determine the Ga ad-dimer bond length and location on Si(100). The Ga ad-dimer height above the Si(400) bulk-extrapolated lattice plane is $h'=P_{400}d_{400}=1.03\pm0.02$ Å. Note that h' was found to be independent of coverage (see Table III). The Ga ad-dimer in-plane location can be confirmed by a consistency check between the P_{220} and P_{400} values. The fact that $P_{220}=(1+P_{400})/2$ indicates that the Ga ad-dimers are centered above one of the 2mm symmetry sites (see Fig. 2). The Ga ad-dimer bond length can also be determined when we combine the (220) and (400) XSW results by using Eqs. (4) and (5). In Eq. (4), the coherent fraction equals the product of the three factors we explained earlier. Among these three factors, the geometrical factor a_H is determined by Eq. (5) since Ga forms symmetric (unbuckled) dimers on Si(100). For each coverage, we found that the ordered fraction C remained unchanged during the time period when both the (400) and (220) XSW measurements were being made. The only unknown remaining in Eq. (4) is the Debye-Waller factor D_H or the thermal vibration amplitude of Ga atoms on the Si(100) surface in the (400) and (220) directions. Here, we make a simplified assumption that the thermal vibrational amplitude is isotropic and is equal to $\langle u^2\rangle^{1/2}=0.12$ Å, a value found by theoretical calculation for the Si(100)-(2×1) surface atoms.[32] This would make $D_{400}=0.86$ and $D_{220}=0.93$ for the Ga atoms. The calculated Ga ad-dimer bond length, $L=2.50\pm0.06$ Å as listed in Table III, is independent of coverage. The error bar of 0.06 Å quoted here in our bond-length measurement includes the uncertainties for the assumption of surface thermal vibrational amplitudes.

TABLE III. Results from XSW measurements for the (400) and (220) reflections. Θ (ML)=Ga coverage; $f_{c,H}$=coherent fraction; P_H=coherent position; h'=Ga-dimer height relative to (400) bulk extrapolated atom planes; $\Delta P=P_{220}-(1+P_{400})/2$; C=Ga ordered fraction; and L=Ga-dimer bond length.

Θ (±0.05)	$f_{c,400}$ (±0.01)	P_{400} (±0.01)	$f_{c,200}$ (±0.01)	P_{220} (±0.01)	h' (Å) (±0.02)	ΔP (±0.02)	C (±0.06)	L (Å) (±0.06)
0.35	0.73	0.76			1.03		0.85	
0.40	0.69	0.75	0.34	0.84	1.02	−0.04	0.80	2.50
0.45	0.67	0.75			1.02		0.79	
0.50	0.55	0.76	0.27	0.88	1.03	0.00	0.64	2.49
0.55	0.54	0.76	0.27	0.88	1.03	0.00	0.63	2.51

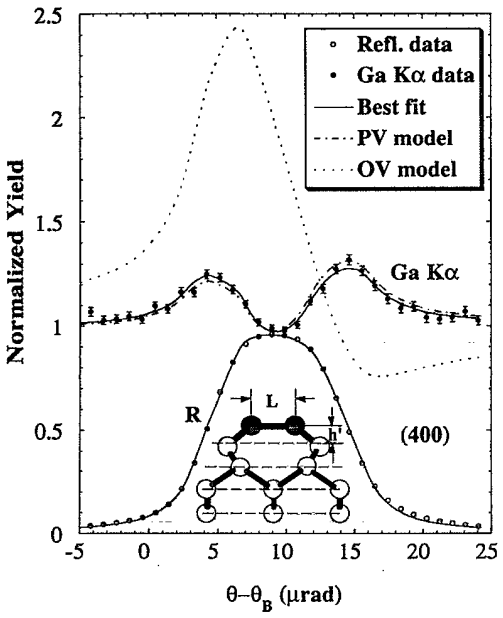

FIG. 5. Experimental data and theoretical curves for the normalized Ga $K\alpha$ fluorescence yield and Si reflectivity R versus Bragg reflection angle θ for the (400) reflection at 13.0 keV. The results of the χ^2 fit of Eq. (3) to the data are listed in Table III. The normalized Ga $K\alpha$ fluorescence yields based on our PV and OV models are also shown. The inset shows the Si atoms as open circles and Ga atoms as filled circles. The dashed lines represent the (400) Miller planes.

VI. DISCUSSION OF THE RESULTS

The total-energy calculations show that the parallel dimer at the valley bridge and between the Si dimer rows (PV model displayed in Fig. 2) has the lowest energy of the four dimer configurations studied. As shown in Table I, the other three dimer structures, namely, OV, OP, and PP, have adsorption energies that are at least 0.7 eV higher than that of the PV model. The orthogonal dimer model at the valley bridge site (OV) which was previously proposed[4] for Ga/Si(100) is found to be the least stable structure. Strong support for the PV model is obtained through a comparison of the calculated dimer height h' of the four models listed in Table I and the XSW measured value, 1.03±0.01 Å. Since the XSW experiment measures the ad-atom height relative to the ideal Si(100)-(1×1) surface, the information listed in Table I can be directly compared to the XSW result. Without considering the Si lattice relaxation, the h' of the PV model is 7% larger than the XSW result, while the other three dimer structures differ by more than 25% with experiment. By including the Si substrate relaxation in the calculation, the h' for the PV structure becomes 1.05 Å (shown in Table II), which is within 2% of the experimental result. Clearly, the PV dimer model is the most favorable structure for the Si(100)-(2×2)-Ga surface—in agreement with previous experimental[10,11] and theoretical studies.[13,14]

To demonstrate the sensitivity of our XSW measurement to the change in Ga height, we compare in Fig. 5 the Ga $K\alpha$ fluorescence yields for the PV and OV models calculated by the DMol method including substrate relaxation with the fluorescence yields of the XSW experimental data and best χ^2 fit of the parametrized yield [Eq. (3)] to the data. It can be easily seen that the fluorescence curves based on our PV model are in excellent agreement with the experimental curves while the OV model curves clearly show different modulations. Typically, the XSW technique can be used to measure coherent positions with a precision of ±0.02 Å. It is therefore an excellent test for theoretical models.

As shown in Table II, the present results on the Si-Si, Ga-Si, and Ga-Ga bond lengths for parallel and orthogonal dimers are in good overall agreement with the pseudopotential calculations of Northrup *et al.*,[13] with the exception of the Ga-Ga bond length for the orthogonal dimer. The Ga-Ga bond length for the parallel dimer from both the DMol and pseudopotential calculations is in reasonable agreement with the XSW result. For both the parallel and orthogonal dimer structures, Ga induces large relaxations of the Si substrate. For example, the first-layer Si atoms have been lifted from −0.38 Å (Ref. 23) to −0.13 and −0.08 Å for the parallel and orthogonal dimers at the valley bridge site, respectively. However, the Si(100) surface still retains the dimerized structure. The present calculation shows that the underlying Si-dimer bond is weakened as a consequence of Ga adsorption. The Si-Si bond length is stretched from 2.23 (Ref. 23) to 2.49 Å which is 6% larger than the bulk Si-Si bond length. In the orthogonal dimer, the Si-Si dimer bond is severely weakened; its bond length is 2.80 Å and is 19% larger. The same trend of Si-Si bond-length stretching is observed in the pseudopotential calculation shown in Table II. This weakening of the Si-Si dimer bond can also be seen in Fig. 6 where the valence charge densities in the Si-dimer plane of the parallel and orthogonal dimer models are shown. For comparison, the charge density of the clean Si(100)-(2×1) surface in the same plane is also displayed. For the parallel dimer [Fig. 6(b)], the covalent bonding between the Si-dimer atoms is easily seen, and this bonding is weaker than in the clean Si surface [Fig. 6(a)]. For the orthogonal dimer [Fig. 6(c)], there are some charge accumulations between the Si-dimer atoms, but apparently the bonding is much weaker than that for the parallel dimer. This will certainly reduce the stability of the orthogonal dimer structure.

When two Ga atoms form a parallel dimer at the valley bridge site, each Ga atom bonds with two top-layer Si atoms and one Ga atom which results in a maximum use of its three valence electrons to form hybridized states with other atoms. This dimer arrangement has the spatial advantage of forming relatively short Ga-Si bonds without seriously disrupting the underlying Si surface. In order to reach a shorter Ga-Si bond length in the case of the orthogonal dimer, the Ga atoms should stay quite close to the Si surface and the Si-Si dimer bond will be greatly stretched. In other words, the Si substrate has to be relaxed significantly to comply with the need to form an orthogonal dimer. We can also see this effect in Fig. 6. For parallel dimers [see Fig. 6(b)], there is a slightly dis-

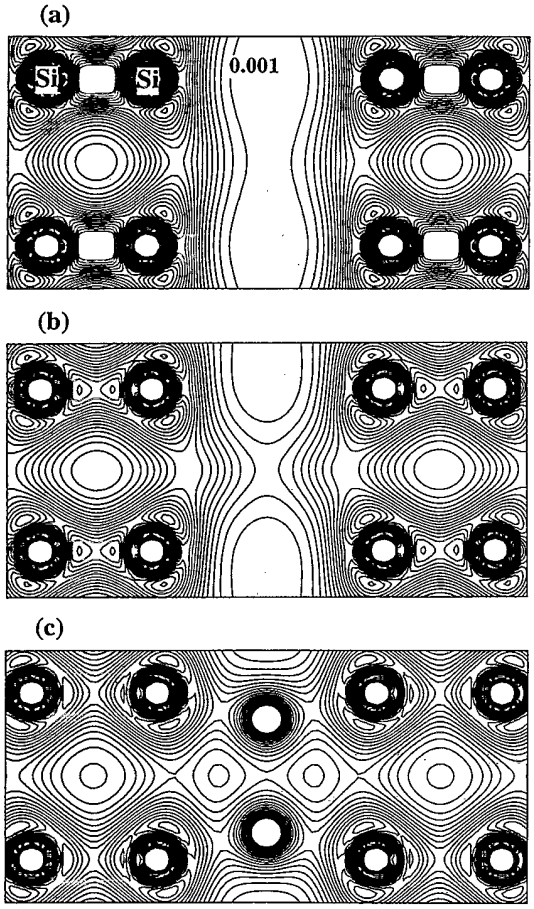

FIG. 6. Contour plots of the valence charge density of Ga/Si(100)-(2×1). The plots are in a (100) plane containing the Si dimers. The contour spacings are 0.004 e/(a.u.)^3. (a) Clean Si(100)-(2×1) surface; (b) parallel dimer, PV; and (c) orthogonal dimer, OV.

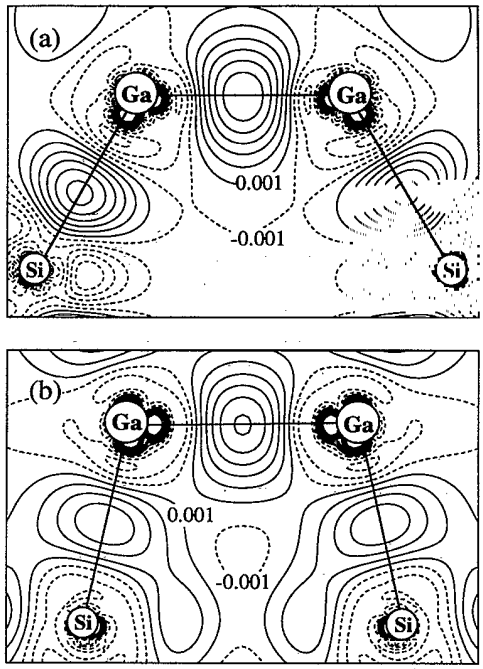

FIG. 7. Contour plots of the deformation charge density for Ga dimer on valley bridge site of Si(100)-(2×1). The plots are in a plane containing both the Ga-Ga dimer and the nearest Ga-Si bond. The contour spacings are 0.002 e/(a.u.)^3. (a) Parallel dimer and (b) orthogonal dimer.

torted charge redistribution in the channel between the Si-dimer row compared to the clean Si surface [shown in Fig. 6(a)]. By contrast, for the orthogonal dimer, in addition to the weakened bonding between Si-Si dimer atoms, there is more charge in the region between Si-dimer rows which indicates that the orthogonal dimer has a stronger influence on the Si surface than the parallel dimer.

Besides the weaker Si-Si bonding in the orthogonal dimer model, the Ga-Si bonding is also weaker than that for the parallel dimer. This is reflected in the larger Ga-Si bond length calculated for the orthogonal dimer (2.63 Å) than for the parallel dimer (2.54 Å) and can be seen in Fig. 7 where the deformation charge density in a plane containing both Ga-Ga and Ga-Si bonds is plotted. The deformation charge density is defined as the difference between the total charge density and the sum of each atomic charge density, so that the bonding between atoms is seen more clearly. The solid contours (positive values) represent charge buildup, or bonding states, and the dashed contours (negative values) stand for charge loss, or antibonding states. For both parallel and orthogonal dimer structures, the covalent bonding between Ga-Ga and Ga-Si is obvious. The fact that more charge accumulates between Ga and Si in the parallel dimer than in the orthogonal dimer again indicates the stronger bonding of Ga-Si in the parallel dimer structure.

Through these analyses of the atomic and electronic structures obtained for the two dimer models, we now know that at least two factors contribute to the stability of the parallel dimer. (i) In a parallel dimer geometry, the Ga dimer induces considerably less distortion on the Si substrate than does the orthogonal dimer, which implies that less work is needed to form a parallel dimer. (ii) The stronger bonding between Ga-Si and Si-Si contributes to the stability of this dimer.

In the parallel dimer structure, we also found that the Si dimers move 0.07 Å towards the center, forming a contracted dimer row configuration, which is indicated by arrows on the PV model shown in Fig. 2. This arrangement of Si dimers was not detected previously in any experiments with group-III metals on Si(100); it is compatible with the 2×2 reconstructed pattern found in LEED experiments. This contracted dimer row results in a shorter Ga-Si bond length and is favorable for the stability of the parallel dimer. It is very possible that the contracted Si dimer row only exists when Ga coverage is below 0.5 ML since greater Ga coverage could destroy the 2×2 structure and force the Si dimer to relax back to its original position.

Finally, we discuss the Ga coverage in forming the 2×2 structure on Si(100)2×1. As shown in Table III, when the Ga coverage is increased from 0.35 to 0.55 ML, the Ga ordered fraction is reduced from 85% to 63%.

However, the Ga ordered coverage defined as $C\Theta$ remains almost constant at about $\frac{1}{3}$ ML. This suggests the increased probability of Ga clustering on the Si(100) when Ga coverage increases. This is consistent with previous STM images[6-8] which show vacancies, missing dimer rows, and antiphase domains on the Ga/Si(100) surface. The fact that the bond lengths and the height of the Ga dimer are insensitive to the change of Ga coverage indicates that the local ordered structure of the Ga dimer on Si(100) remains the same up to $\frac{1}{2}$ ML.

VII. CONCLUSION

We have investigated Ga adsorption on the Si(100)-(2×1) surface at low coverage by a combination of first-principles molecular-cluster approach and the x-ray standing-wave measurement. Four possible Ga-dimer structures calculated using cluster models with 33 and 37 atoms show that the parallel dimer in between two Si-dimer rows gives the lowest energy. Using cluster models containing 75 and 77 atoms, we further calculated the relaxation of the Si substrate when a parallel dimer or an orthogonal dimer is present. By comparing the calculated results and the XSW measurement, it is concluded that the parallel dimer model can be used to interpret the Si(100)-(2×2)-Ga surface structure at coverages below one-half monolayer. This agrees with the pseudopotential calculation by Northrup *et al.*,[13] who also found that the parallel dimer model is strongly favored over the orthogonal dimer. The stability of the parallel dimer over the orthogonal dimer is explained based on an analysis of atomic bonding and Si substrate relaxation. Our study shows that combining state-of-the-art theoretical approaches and sophisticated experimental techniques leads to a more complete understanding of the interface structure.

ACKNOWLEDGMENTS

We thank J. Nogami, J. E. Northrup, and J. R. Patel for helpful discussions. This work was supported by the MRL Program of the National Science Foundation, at the Materials Research Center of Northwestern University, under Award No. DMR-9120521, and by the U.S. Department of Energy under Contract No. W-31-109-ENG-38 to ANL, Contract No. DE-AC02-76CH00016 to NSLS and Contract No. DE-FG02-89ER-45399 to HU, and by a computing grant from the National Center for Supercomputing Applications, Urbana/Champaign, Illinois.

[1]D. Haneman, Rep. Prog. Phys. **50**, 1045 (1987), and references therein.
[2]D. H. Rich, A. Samsavar, T. Miller, H. F. Lin, and T.-C. Chiang, Phys. Rev. Lett. **58**, 579 (1987).
[3]T. Sakamoto and H. Kawanami, Surf. Sci. **111**, 177 (1981).
[4]H. Bourguignon, K. L. Carleton, and S. R. Leone, Surf. Sci. **204**, 455 (1988).
[5]H. Bourguignon, R. V. Smilgys, and S. R. Leone, Surf. Sci. **204**, 473 (1988).
[6]J. Nogami, Sang-il Park, and C. F. Quate, Appl. Phys. Lett. **53**, 2086 (1988).
[7]A. A. Baski, J. Nogami, and C. F. Quate, J. Vac. Sci. Technol. A **8**, 245 (1990).
[8]J. Nogami, A. A. Baski, and C. F. Quate, J. Vac. Sci. Technol. A **8**, 3520 (1990).
[9]J. Nogami, A. A. Baski, and C. F. Quate, Phys. Rev. B **44**, 1415 (1991).
[10]B. E. Steele, L. Li, J. L. Stevens, and L. S. T. Tsong, Phys. Rev. B **47**, 9925 (1993).
[11]H. Itoh, J. Itoh, A. Schmid, and T. Ichinokawa, Phys. Rev. B **48**, 14 663 (1993).
[12]I. P. Batra, Phys. Rev. Lett. **63**, 1704 (1989).
[13]J. E. Northrup, M. C. Schabel, C. J. Karlsson, and R. I. G. Uhrberg, Phys. Rev. B **44**, 13 799 (1991).
[14]G. Brocks, P. J. Kelly, and R. Car, Phys. Rev. Lett. **70**, 2786 (1993).
[15]E. Fontes, J. R. Patel, and F. Comin, Phys. Rev. Lett. **70**, 2790 (1993).
[16]P. Krüger and J. Pollmann, Phys. Rev. Lett. **72**, 1130 (1994); E. Fontes, J. R. Patel, and F. Comin, *ibid.* **72**, 1131 (1994).
[17]R. I. G. Uhrberg, R. D. Bringans, R. Z. Bachrach, and J. E. Northrup, Phys. Rev. Lett. **56**, 520 (1986).
[18]M. Richter, J. C. Woicik, J. Nogami, P. Pianetta, K. E. Miyano, A. A. Baski, T. Kendelewicz, C. E. Bouldin, W. E. Spicer, C. F. Quate, and I. Lindau, Phys. Rev. Lett. **65**, 3417 (1990).
[19]S. Tang and A. J. Freeman, Phys. Rev. B **48**, 8068 (1993).
[20]B. Delley, J. Chem. Phys. **92**, 508 (1990), and references therein.
[21]B. Delley, J. Chem. Phys. **94**, 7245 (1991).
[22]L. Hedin and B. I. Lundqvist, J. Phys. C **4**, 2064 (1971).
[23]S. Tang, A. J. Freeman, and B. Delley, Phys. Rev. B **45**, 1776 (1992).
[24]S. Tang and A. J. Freeman, Phys. Rev. B **47**, 1460 (1993).
[25]B. W. Batterman, Phys. Rev. **133**, A759 (1964); Phys. Rev. Lett. **22**, 703 (1969).
[26]P. L. Cowan, J. A. Golovchenko, and M. F. Robbins, Phys. Rev. Lett. **44**, 1680 (1980).
[27]J. A. Golovchenko, J. R. Patel, D. R. Kaplan, P. L. Cowan, and M. J. Bedzyk, Phys. Rev. Lett. **49**, 560 (1982).
[28]M. J. Bedzyk and G. Materlik, Phys. Rev. B **31**, 4110 (1985).
[29]L. E. Berman, B. W. Batterman, and J. M. Blakely, Phys. Rev. B **38**, 5397 (1988).
[30]J. Zegenhagen, Surf. Sci. Rep. **18**, 199 (1993), and references therein.
[31]A. Ishizaka and Y. Shiraki, J. Electrochem. Soc. **133**, 666 (1986).
[32]O. L. Alerhand, J. D. Joannopoulos, E. J. Mele, Phys. Rev. B **39**, 12 622 (1989).